

Measurement of long-range wavefunction correlations in an open microwave billiard

Y.-H. Kim,¹ U. Kuhl,¹ H.-J. Stockmann,¹ and P.W. Brouwer²¹Fachbereich Physik der Philipps-Universität Marburg, Renthof 5, D-35032 Marburg, Germany²Laboratory of Atomic and Solid State Physics, Cornell University, Ithaca, New York 14853-2501, USA

(Dated: March 22, 2024)

We investigate the statistical properties of wavefunctions in an open chaotic cavity. When the number of channels in the openings of the billiard is increased by varying the frequency, wavefunctions cross over from real to complex. The distribution of the phase rigidity, which characterizes the degree to which a wavefunction is complex, and long-range correlations of intensity and current density are studied as a function of the number of channels in the openings. All measured quantities are in perfect agreement with theoretical predictions.

PACS numbers: 73.23.-b, 73.23.Ad, 05.45.Mt, 72.20.-i

From a statistical point of view, eigenvalues and eigenfunctions of the wave equation in a chaotic billiard are well described by random matrix theory [1]: Depending on the presence or absence of time-reversal symmetry, they show the same distribution as eigenvalues and eigenvectors of a large hermitian matrix with random Gaussian distributed real or complex elements. Whereas random matrix theory predicts a very characteristic eigenvalue distribution [1] with eigenvalue repulsion and spectral rigidity [2], its predictions for eigenvectors are rather "uninteresting": eigenvector elements are independent Gaussian distributed real or complex random numbers.

The situation is different for the eigenvectors of a random matrix that interpolates between the standard ensembles with real and complex matrix elements. An example of such an interpolating ensemble is the "Pandey-Mehta-Hamiltonian" [3]

$$H(\gamma) = H_0 + \gamma H_1; \quad (1)$$

where H_0 and H_1 are real and complex random hermitian matrices, respectively, and γ is a crossover parameter. For such an interpolating random matrix ensemble the eigenvector elements have a non-Gaussian distribution [4, 5] and acquire correlations, both between elements of the same eigenvector [6, 7] and between different eigenvectors [8].

Experimental verification of this eigenvector distribution has proven problematic because the long-range correlations and the deviations from Gaussian distributions are only of the order of a few percent [4, 5, 6, 7, 8]. An additional complication arises from the fact that the crossover parameter needs to be fitted to the experiment. These complications may explain why measurements of wavefunction distributions in two-dimensional microwave cavities in which time-reversal symmetry was broken using magneto-optical effects were inconclusive with respect to the functional form of the probability distribution and did not reveal long-range wavefunction correlations [9].

An alternative method to observe the real-to-complex crossover is to consider traveling waves in a billiard that is opened to the outside world [10]. For microwaves, such an open billiard is obtained by connecting a two-dimensional microwave cavity to waveguides. The parameter governing the crossover from real to complex wavefunctions is the total number of channels N in the two waveguides. As was shown by one of the authors [11], wavefunctions in this crossover have a non-Gaussian distribution and long-range correlations, just like the eigenvectors of the Pandey-Mehta-Hamiltonian (1). The main difference, however, is that the crossover parameter N is discrete and can be measured independently. This allows a γ -parameter free comparison of theory and experiment.

We here report on the first measurement of such long-range wavefunction correlations in the real-to-complex crossover. The basic principles of the experiment can be found in Ref. 12. We used a rounded rectangular cavity (21 cm \times 18 cm) coupled to two waveguides of width 3 cm with a cut-off frequency at $\gamma_c = 5$ GHz. To break the symmetry of the shape of the resonator and to block direct transport, two half disks with a radius of 3 cm were placed in the resonator. To avoid unwanted reflection, absorbers were placed at the end of the leads. We scanned the billiard on a square grid of 5 mm with a movable antenna A_1 and measured transmission S_{12} in the range of 4–18 GHz from a fixed antenna A_2 in the end of the right lead. The fixed antenna had a metallic core of diameter 1 mm and a teflon coating while the probe antenna A_1 was a thin wire of diameter 0.2 mm to minimize the leakage current. The lengths of the antenna A_1 and antenna A_2 were 4 and 5 mm respectively.

For microwave frequencies $\omega < \omega_{\max} = c/2d = 18.75$ GHz, where c is the velocity of light and d is the resonator height, the billiard is quasi-two-dimensional. In this regime there is an exact correspondence between electrodynamics and quantum mechanics, where the component of the electric field perpendicular to the plane of the microwave billiard E_z corresponds to the quantum-mechanical wave function ψ . We normalize the wavefunction such that $\int |\psi(\mathbf{r})|^2 d\mathbf{r} = 1$. Then the

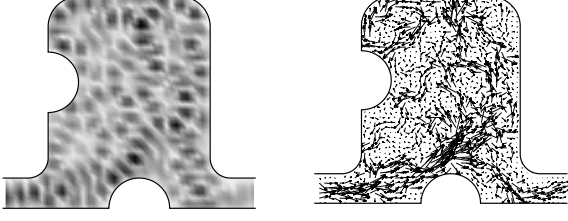


FIG. 1: Left panel: Grey scale plot of measured intensity $|\psi|^2$ at $\omega = 12.015$ GHz. Black corresponds to maximum intensity. Right panel: Measured current density for the same wave function. Arrow lengths indicate the magnitude of the Poynting vector.

square of the electric field and the Poynting vector map to the normalized "intensity" and "current density", respectively,

$$I(\mathbf{r}) = A |\psi(\mathbf{r})|^2; \quad \mathbf{j}(\mathbf{r}) = \frac{A}{k} \text{Im} [\psi(\mathbf{r}) \nabla \psi(\mathbf{r})]; \quad (2)$$

where A is the area of the billiard and k the wavenumber. Figure 1 show typical intensity and current patterns thus obtained.

The correspondence between the perpendicular component of the electric field E_z and the wavefunction has been used previously to study the spatial distributions and correlation functions of currents and vortices in open billiards [13, 14]. In the present work we study spatial correlation functions of the squares of intensities and currents. The statistical average is taken by averaging over both position and frequency. It is for these quantities and for this full ensemble average that long-range correlations were predicted [11]. Before we describe the experimental results, we briefly summarize the conclusions of Ref. 11.

In Ref. 11 the wavefunction distribution was described as the convolution of a Gaussian distribution with correlated real and imaginary parts and that of a single complex number, the dot product of the wavefunction and its time reversed,

$$\psi(\mathbf{r}) = \int d\mathbf{r}' \psi(\mathbf{r}') \psi(\mathbf{r}'), \quad (3)$$

The absolute value $|\psi|^2$ is known as the "phase rigidity" of [7]. The Gaussian wavefunction distribution at a fixed value of ω implies a generalized Porter-Thomas distribution for the intensity,

$$P(I) = \frac{1}{\sqrt{I}} \exp\left(-\frac{I}{I_0}\right) \frac{1}{I_0} \frac{1}{\sqrt{I}}; \quad (4)$$

so that the full intensity distribution is obtained by convolution of Eq. (4) and the distribution $p(\omega)$ of ω ,

$$P(I) = \int d\omega p(\omega) P(I|\omega); \quad (5)$$

The distribution $p(\omega)$ was calculated in Ref. 11 using random matrix theory.

In order to explain the origin of long-range correlations of intensity and current density in an open chaotic billiard, we consider the joint distribution of intensities at points \mathbf{r} and \mathbf{r}' with separation $k|\mathbf{r} - \mathbf{r}'| \gg 1$,

$$P[I(\mathbf{r}); I(\mathbf{r}')] = \int d\psi p(\psi) P[I(\mathbf{r})|\psi] P[I(\mathbf{r}')|\psi]; \quad (6)$$

For an open billiard, ψ has a nontrivial distribution, hence the long-range correlations of $P[I(\mathbf{r}); I(\mathbf{r}')]$. Whereas random matrix theory predicts the long-range correlations of intensities through Eq. (6), it cannot alone predict the long-range correlations of current densities and the precise dependence of these correlators on the separation $|\mathbf{r} - \mathbf{r}'|$ for $k|\mathbf{r} - \mathbf{r}'|$ of order unity. However, as shown in Ref. 11, the latter can be obtained from the random matrix result by making use of Berry's ansatz [15], which expresses ψ as a random sum over plane waves,

$$\psi(\mathbf{r}) = \sum_{\mathbf{k}} a(\mathbf{k}) e^{i\mathbf{k} \cdot \mathbf{r}}; \quad (7)$$

Here the plane wave amplitudes $a(\mathbf{k})$ have a Gaussian distribution with zero mean and with variance

$$\langle a(\mathbf{k}) a(\mathbf{k}') \rangle = \langle a(\mathbf{k}) a(\mathbf{k}) \rangle \delta(\mathbf{k} - \mathbf{k}'); \quad (8)$$

where θ is the (random) phase rigidity of ψ . Performing the ensemble average using Eqs. (7) and (8), correlators of intensity and current density are then expressed in terms of moments of the phase rigidity θ^2 . Long range correlations are found for correlators involving the square of the intensity and the current density,

$$\begin{aligned} \langle I(\mathbf{r})^2 I(\mathbf{r}')^2 \rangle_c &= \langle \text{var} |\psi|^2 + 4f^2 h_4 + 13j^2 |\psi|^2 + j^4 \rangle_i \\ &\quad + 4f^4 h_1 + 4j^2 |\psi|^2 + j^4 \rangle_i; \\ \langle I(\mathbf{r})^2 \mathbf{j}(\mathbf{r}')^2 \rangle_c &= \frac{1}{4} \langle \text{var} |\psi|^2 + f^4 h_2 - j^2 |\psi|^2 + j^4 \rangle_i; \\ \langle \mathbf{j}(\mathbf{r})^2 \mathbf{j}(\mathbf{r}')^2 \rangle_c &= \frac{1}{4} \langle \text{var} |\psi|^2 + \frac{1}{2} f^2 h_1 - 2j^2 |\psi|^2 + j^4 \rangle_i \\ &\quad + \frac{1}{4} f^4 h_3 - 5j^2 |\psi|^2 + 2j^4 \rangle_i; \end{aligned} \quad (9)$$

Here $f = J_0(k|\mathbf{r} - \mathbf{r}'|)$, J_0 being the Bessel function, and the subscript "c" refers to the connected correlator, $\langle A B \rangle_c = \langle A B \rangle - \langle A \rangle \langle B \rangle$. The relevant moments of the phase rigidity θ^2 were calculated in Ref. 11: For $N = 2, 4$, and 6 , one has $\langle \theta^2 \rangle = 0.7268, 0.5014$, and 0.3918 , and $\langle \theta^4 \rangle = 0.6064, 0.3285$, and 0.2155 , respectively.

We now describe the measured wavefunction distributions. We first discuss wavefunction distributions measured at a fixed frequency, and compare to the theory for the corresponding fixed value of θ . A statistical distribution at a fixed frequency is obtained by varying the position of the antenna only. The phase rigidity θ^2 can be measured independently using Eq. (3). Fig. 2

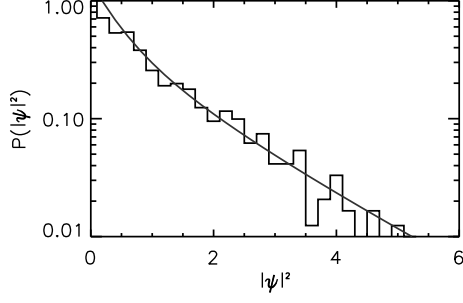


FIG. 2: Intensity distribution for the wave function at $\omega = 12.015$ GHz. Theoretical values from Eq. (4) are plotted with solid line.

shows the intensity distribution for the intensity pattern shown in the left panel of Fig. 1 together with the theory of Eq. (4), using the measured value of $j^2 = 0.5202$. As was discussed in Ref. 13, there are frequency regimes where the leakage to the probe antenna becomes intolerably high, either due to the fact that the transport through the cavity is small, or due to some strongly scarred wave functions. In all such cases there were strong deviations from the generalized Porter-Thomas behavior described by Eq. (4). We therefore only used frequency regimes where $P(j^2)$ was in agreement with theory on a confidence level of 90 percent. To have a well defined number of transversal modes within each waveguide, we investigate the frequency regimes 5–9.5, 10–14.5, 15–18 GHz, corresponding to a total number of channels $N = 2, 4, 6$, respectively (i.e., 1, 2, and 3 propagating modes in each waveguide)

We now describe our results for a full ensemble average, in which both the position of the detector antenna and the frequency are varied. Fig. 3 shows the measured phase rigidity distribution $P(j^2)$ together with the theory of Ref. 11, for $N = 2, 4$, and 6. Good agreement is found between experiment and theory, especially as there is no free parameter. Figures 4, 5, and 6 show measurement and theoretical prediction for the correlation functions of the squared intensity and the squared current density at positions r and r^0 . Since these correlation functions depend on the positions r and r^0 through the combination $k|r - r^0|$ only, results from different frequency regimes can be superimposed by a proper scaling. In our analysis, we selected frequency windows for averaging of $\omega = 0.3$ GHz guaranteeing that $c = 2L$, where L is the billiard size and c the velocity of wave propagation. The gaps in the $N = 4, 6$ histograms for small values of $k|r - r^0|$ reflect the spatial resolution limited to 5 mm due to the chosen grid size. For the long-range correlations, we observe excellent agreement between experiment and theory. The short-range oscillations predicted by theory are suppressed to a large extent in the experiment for the correlators that involve the current density, however.

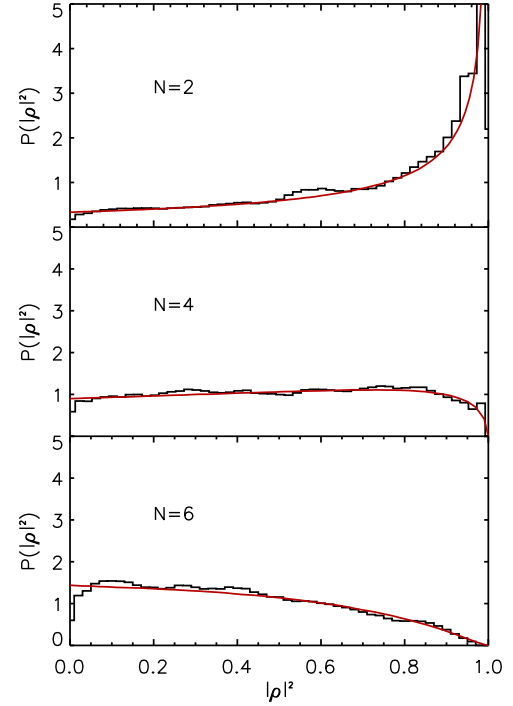


FIG. 3: Phase rigidity distribution $P(j^2)$ for different values of the total number of channels N . Solid curves indicate the theory of Ref. 11.

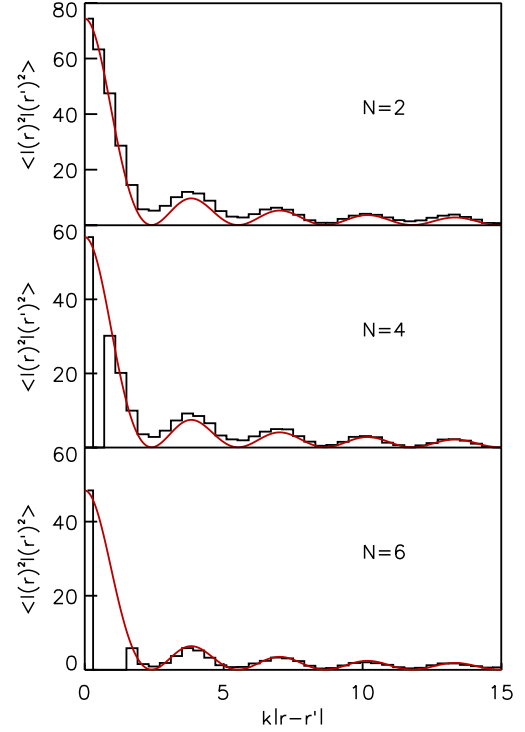


FIG. 4: Connected correlator of squared intensity $\langle I(r)^2 I(r^0)^2 \rangle_c$ versus $k|r - r^0|$ for different values of the total number of channels N .

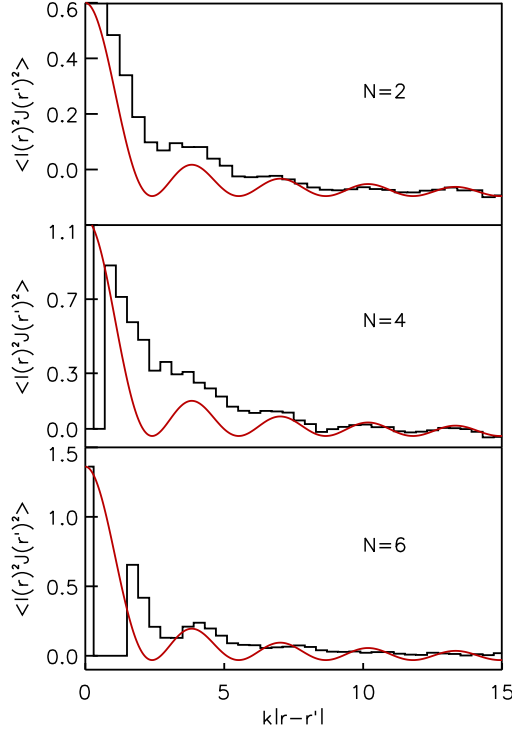


FIG. 5: Connected correlator of squared intensity and squared current density $\langle I(r)^2 J(r^0)^2 I_c \rangle$ versus $|r-r^0|$, for different values of the total number of channels N .

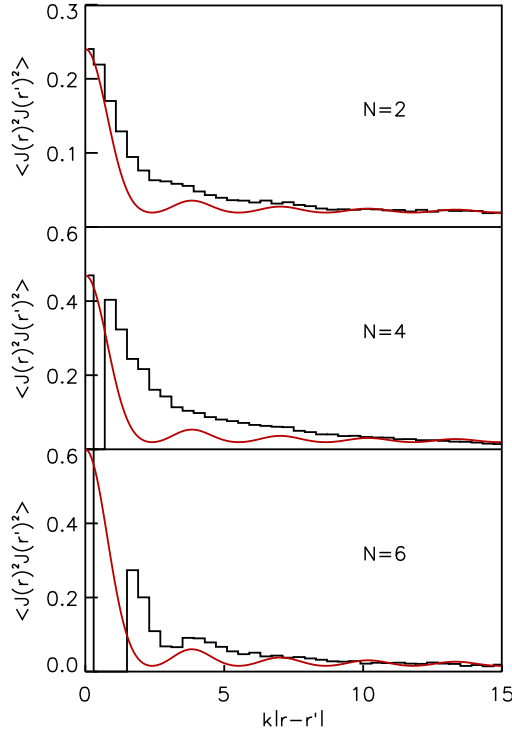


FIG. 6: Connected correlator of squared current density $\langle J(r)^2 J(r^0)^2 I_c \rangle$ versus $|r-r^0|$ for different values of the total number of channels N .

This, again, is a consequence of the limited resolution. We would like to stress, however, that the asymptotic values of all correlations in the limit $|r-r^0| \rightarrow \infty$ is different from zero and in perfect agreement with the predictions from Eq. (9).

Long-range correlations have also been observed in the transmission of microwaves [16] and visible light [17] through two- and three-dimensional disordered media, in which wave propagation is diffusive. There are important differences between the long-range correlations observed in Refs. 16, 17 and those in ballistic systems, which are reported here. First, in Refs. 16, 17, long-range correlations appear already for the intensity autocorrelation function, whereas we find long-range correlations for correlators of second and higher moments only. Second, in Refs. 16, 17, the correlations scale with the inverse of the sample conductance, whereas in the present work there is no small parameter that sets the size of the long-range correlations, irrespective of sample size or distance. In that sense, only the latter correlations are truly long range.

This work was supported by the DFG, the NSF under Grant No. DMR-0334499 and by the Packard foundation (P.W.B.).

-
- [1] T. Guhr, A. M. Müller-Groeling, and H. A. Weidenmüller, Phys. Rep. 299, 189 (1998).
 - [2] M. L. Mehta, Random Matrices (Academic Press, 1991), 2nd ed.
 - [3] A. Pandey and M. L. Mehta, Commun. Math. Phys. 87, 449 (1983).
 - [4] H.-J. Sommers and S. Idia, Phys. Rev. E 49, 2513 (1994).
 - [5] V. I. Fal'ko and K. B. Efetov, Phys. Rev. B 50, 11267 (1994).
 - [6] V. I. Fal'ko and K. B. Efetov, Phys. Rev. Lett. 77, 912 (1996).
 - [7] S. A. van Langen, P. W. Brouwer, and C. W. J. Beenakker, Phys. Rev. E 55, 1 (1997).
 - [8] S. Adam, P. W. Brouwer, J. P. Sethna, and X. Waintal, Phys. Rev. B 66, 165310 (2002).
 - [9] S.-H. Chung, A. Gokim, D.-H. Wu, J. S. A. Bridgewater, E. Ott, T. M. Antonsen, and S. M. Anlage, Phys. Rev. Lett. 85, 2482 (2000).
 - [10] R. Pnini and B. Shapiro, Phys. Rev. E 54, 1032 (1996).
 - [11] P. Brouwer, Phys. Rev. E 68, 046205 (2003).
 - [12] U. Kuhl, E. Persson, M. Barth, and H.-J. Stockmann, Eur. Phys. J. B 17, 253 (2000).
 - [13] M. Barth and H.-J. Stockmann, Phys. Rev. E 65, 066208 (2002).
 - [14] Y.-H. Kim, M. Barth, U. Kuhl, and H.-J. Stockmann, Prog. Theor. Phys. Suppl. 150, 105 (2003).
 - [15] M. V. Berry, J. Phys. A 10, 2083 (1977).
 - [16] P. Sebbah, B. Hu, A. Genack, R. Pnini, and B. Shapiro, Phys. Rev. Lett. 88, 123901 (2002).
 - [17] V. Emiliiani, F. Intonti, M. Cazayous, D. Wiersma, M. Colocci, F. Aliev, and A. Lagendijk, Phys. Rev. Lett. 90, 250801 (2003).